Tampere University

Dang Trieu

DESIGN OF TUNNEL DIODE-BASED REFLECTION AMPLIFIER

A SPICE-based implementation

Bachelor Thesis
Faculty of Information Technology and Communication Sciences
Examiner: Professor Matti Mäntysalo
June 2024

ABSTRACT

Dang Trieu: Design of tunnel diode-based reflection amplifier
Bachelor Thesis
Tampere University
Bachelor of Science and Engineering
June 2024

RFID is a powerful technology that made contactless payments and access cards possible, as well as provided solutions to many industrial processes involving counting, tracking, and locating. In combination with state-of-the-art electronics printing technology, an RFID tag can potentially be integrated into a flexible thin-film sensor module, realizing many applications in bio-tracking, wildlife monitoring, etc.

In order to maintain their ultra-compact design and cheap manufacturing cost, RFID systems take advantage of the backscatter communication architectures. By reflecting incident RF signal to convey information instead of generating its own carrier, power-hungry active components can be eliminated from the circuit, and batteries can be replace by ambient energy harvesters. As the key part of any backscattering system, the reflection amplifier plays a vital role in tag-to-reader communication.

This work revisits the proposed idea of exploiting quantum tunneling effect using the tunnel diode in a reflection amplifier for high gain and low bias power, providing a starting point for the design process. The performance of the tunnel diode-based reflection amplifier are then demonstrated in a simulation.

Keywords: Backscatter communication, Reflection amplifier, Tunnel diode, Circuit design, SPICE model

PREFACE

Working on this thesis has been a uniquely tough mental and academic challenge. It takes an unprecedented degree of self-discipline and time-management for me to complete this project, and through that I have learnt a lot about myself, and about this incredibly interesting topic. I would like to express my deepest gratitude toward professor Matti Mäntysalo for the opportunity to work on this research, and for his support throughout the duration of this thesis work. I would also like to thank my lovely fuksi Erica for introducing me to the right person at the perfect moment.

I want to thank the program coordinators Tiina and Laetecia, my tutors, my teacher tutor Lucie, and all my wonderful friends for just being there since day one and making my years at Tampere University an amazing time. All of you have broken me out of my shell, and thanks to that I have enjoyed life in ways I could have never imagined before.

Finally, I want to thank my family and my friends in Vietnam for their constant support. I would also like to thank you, my reader. I hope you enjoy your reading.

Tampere, 4th June 2024

Dang Trieu

CONTENTS

LIST OF FIGURES

LIST OF TABLES

LIST OF SYMBOLS AND ABBREVIATIONS

GaAs	Gallium arsenide
Ge	Germanium
InP	Indium phosphide
ADS	Advance Design System - a circuit design software
BCS	Backscatter communication system
BJT	Bipolar junction transistor
BLE	Bluetooth Low Energy
CW	Continuous wave
DC	Direct-current
FET	Field-effect transistor
IoT	Internet of Things
LoRa	Long Range - a radio communication technique
MESFET	Metal-semiconductor field-effect transistor
MOSFET	Metal-oxide-semiconductor field-effect transistor
NDR	Negative differential resistance
PCB	Printed circuit board
RF	Radio-frequency
RFID	Radio-frequency identification
VCCS	Voltage-controlled current source

1. INTRODUCTION

Radio Frequency Identification, commonly abbreviated as RFID, has reshaped our daily tasks in many ways. It allows the seamless flow of cash directly from one's bank account to their purchases with a light tap, eliminating the needs for physical money. It allows one to access multiple doors within the same system using a single key card, and also simplifies door access management. RFID-based item tracking systems can be found in warehouses and supermarkets, helping with counting, locating, and restocking [1].

Utilizing electronic printing methods, an integration of RFID tags and sensor modules enabled by ambient energy harvesters can be embedded on thin and flexible substrates such as paper or other polymer-based materials. Such innovation can open a vast horizon of possibilities in Internet of Things (IoT), bio-monitoring, nutrition measuring, "smart skin", etc. [2], [3]. Additive electronics printing technology produces virtually no byproduct, while being able to realize designs of up to micrometer-scale resolution, and paper-based substrates are low-cost and environmentally friendly. These properties makes printed RFID a strong candidate for sustainable and easy-to-scale next-generation electronics. [2]

RFID refers to a short-range wireless communication system consisting of readers and tags. When a tag reaches the close proximity of a reader, a brief connection is established between the two devices, in which identification codes and/or other relevant information, can be exchanged [4]. Such systems operate on the basis of backscatter communication, utilizing the typically-unwanted reflection of signal to transmit data. The reflection amplifier plays a key role in backscatter communication as it allows the modulation of the reflected signal.

This work looks into a proposed high-gain low-power reflection amplifier design utilizing the quantum tunneling effect [5] using tunnel diodes, which are very rare and costly in the market due to their difficult fabrication process, inconsistent performance, and their requirement of expensive scarce materials such as Germanium and Gallium. This research is done in parallel with an attempt of the Laboratory for Future Electronics [6] to fabricate tunnel diodes using solution processable technologies. The objective of this thesis is to provide a starting point for the design process of the reflection amplifier that can be implemented, in addition to other components, on a fully functional printed RFID tag.

Structure of the thesis

Expanding from the context provided in this chapter, chapter 2 introduces the necessary background knowledge and presents several related works. Chapter 3 describes the steps taken and methods utilized to achieve an initial design of the reflection amplifier. Chapter 4 explains the simulation setup, present the results, as well as their implications and simulation-based tweaking possibilities. Finally, chapter 5 summarizes the findings and concludes the thesis.

2. BACKGROUND

The first step in the making of this thesis was to gather from available literature the necessary background theory for the tunnel diode-based reflection amplifier. Section 2.1 provides a brief introduction to backscatter communication. Section 2.2 delves into the reflection amplifiers, including their design theory and a comparison table between existing works. Finally, an introduction to the tunnel diode is given in section 2.3 to provide the reason why these components can be used in the amplifiers, as well as their limitations.

2.1 Backscatter communication

Backscatter communication is a communication technology that takes advantage of the reflection of signal, which is usually an unwanted phenomenon that affects signal integrity. The defining characteristic of a backscattering node is that it does not generate radio-frequency (RF) carrier wave on its own; instead, it sends information-carrying signals by reflecting at different gain levels an incident RF continuous wave (CW) emitted by an external source. The external CW source can be either a reader, a dedicated RF wave emitter (carrier emitter), or an ambient RF source (e.g., cellular base stations, TV towers, Wi-Fi access point). Figure 2.1 shows different backscatter communication system (BCS) architectures [7]. Outsourcing the carrier wave eliminates power-hungry active components from the RFID tags, allowing compact circuitry that can be sufficiently powered with ambient energy harvesting technology [8].

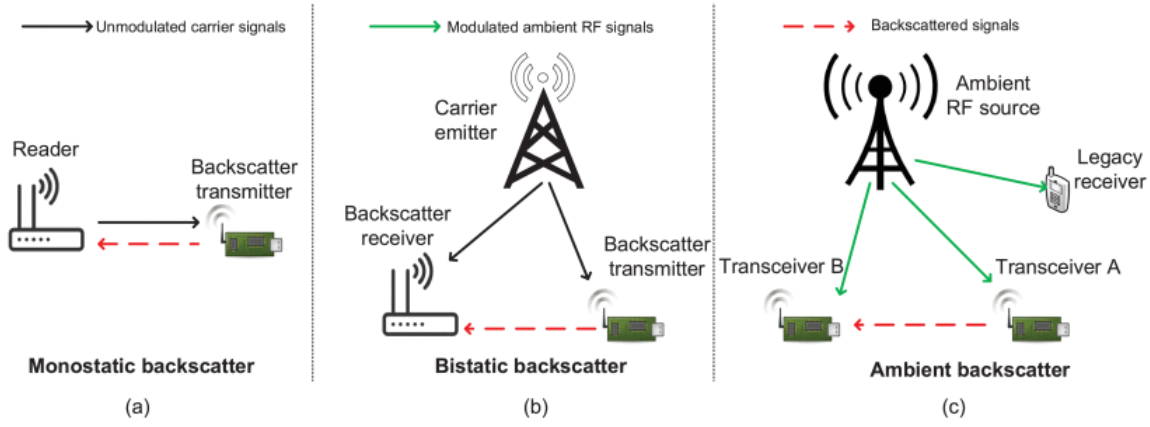

Figure 2.1. *Classification of backscatter communication systems*

A monostatic BCS consists of readers and mobile backscattering nodes, i.e. tags [9]. The architecture of a tag includes an RF energy-harvesting block, a battery, a modulation block, and an information decoder, as illustrated in Figure 2.2 [9]. The tag relies on the incident CW radiated from the reader to power itself using the energy harvester. On the other hand, the reader has its own power supply (e.g. power grids or high-capacity batteries) in addition to a full set of conventional RF components, allowing it to generate and emit a carrier CW, transmit information, and process received signal [9].

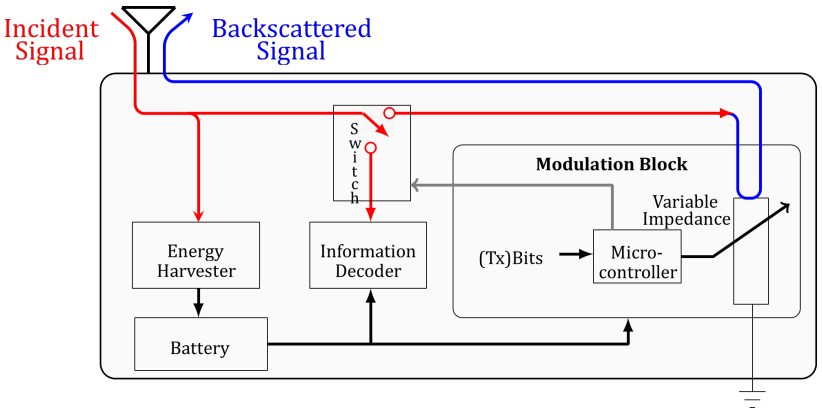

Figure 2.2. *The architecture of a backscattering tag*

There are two modes of communication in a monostatic BCS: forward information transmission, i.e. reader-to-tag communication, and backward information transmission, i.e. tag-to-reader communication [9]. In forward information transmission, the reader emits intensity-modulated wave that can be demodulated by the tag based on energy-detection, and then translated in the information decoded block. In the latter communication mode, the reader emits a single-tone CW, which is reflected as well as modulated by the modulation block of the tag. The microcontroller alternates between different reflection coefficient values through the variable impedance to modulate the reflected signal in both amplitude and phase.

The tags architecture is shared between all BCS topologies, but different external CW sources are utilized. In bistatic BCSs, dedicated carrier emitters are installed at critical positions to produce the necessary CW for the tags; in ambient BCSs, the incident waves are taken from already-existing RF wave emitters such as TV towers or Wi-Fi access points. In such BCS approaches, the range over which information from the tags can be accessed is greatly increased, potentially enabling tag-to-tag communication. Hence, these architectures can be the basis of low-power battery-free IoT systems, offering even more scalability for the implementations of smart home and factory management. However, there are still lots of challenges to be addressed in order for backscatter communication to even level with conventional solutions. They includes the limitations in tags communication range, their signal integrity, energy harvesting efficiency, as well as cyber security [10].

2.2 Reflection amplifier

The reflection coefficient of a signal transmission line refers to the ratio between the reflection and the input signal as a consequence of impedance discontinuity. This phenomenon is causes lossy transmission line, and introduces distortion. A reflection amplifier is a one-port device that leverages the reflection of signal by mismatching the input impedance and the load impedance. When a sinusoidal signal within the desired frequency range at a certain power level is fed to its input through an antenna, a higher amplitude signal with the same frequency exits through the same port, transformed into electromagnetic wave by the same antenna. Such features are achieved in state-of-the-art reflection amplifier designs by using RF transistors or using nonlinear components with negative differential resistance at certain DC bias voltage, such as tunnel diodes and Gunn diodes [11] [12] [13] to maximize the reflection coefficient. A general block diagram of a negative resistance reflection amplifier is shown in Figure 2.3 [13].

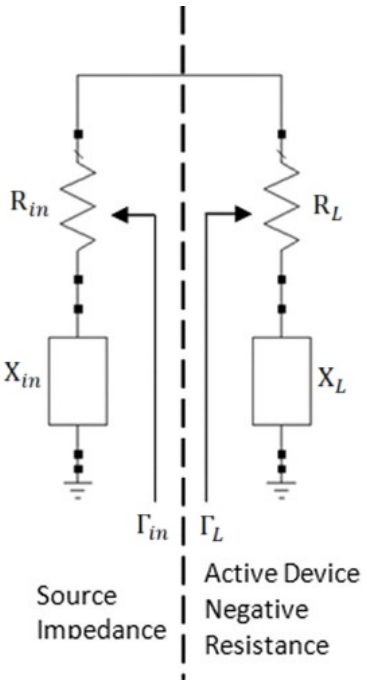

Figure 2.3. *Block diagram of a one port reflection amplifier*

The negative load impedance Z_L of a reflection amplifier biased with DC voltage V_{bias} receiving input signal with RF power P_{in} at frequency f_{in} can be expressed as:

$$Z_L(f_{in}, V_{bias}, P_{in}) = -R_L + jX_L, \quad R_S > 0 \tag{2.1}$$

The reflection coefficient $|\Gamma_S|$ of the amplifier is given in [13] as:

$$|\Gamma_S| = |\frac{Z_{in} - Z_L}{Z_{in} + Z_L}| \tag{2.2}$$

The reflection coefficient maximizes for an input RF power at the resonating frequency where the impedance of the reflection amplifier matches with the input impedance such that $Z_{in}(f_{in}, P_{in}) + Z_L(f_{in}, P_{in}) = 0$. Practically, the reflection gain is limited by the low power output of the DC biasing source, which make an infinite gain impossible even with the perfect impedance matching. One can optimize the performance of a reflection amplifier by matching impedance at the desired frequency and input RF power.

Reflection amplifier is not a novel concept, many designs utilizing various components such as BJTs, FETs, MOSFETs, as well as tunnel diodes to reach negative resistance values have been proposed throughout the last two decades. Table 2.1 (adopted from [12]) compares the operation parameters of the proposed reflection amplifiers and their performances in terms of power consumption, gain, and power-added efficiency (η). Recent works tend to explore implementations of tunneling reflection amplifier. Despite using significantly lower DC bias voltage V_{dc} and thus lower bias power P_{dc}, these amplifiers can have gains that are comparable to the matured transistor-based reflection amplifiers.

Table 2.1. *Comparison of State-of-the-art reflection amplifiers available in literature*

Ref.	Year	Device	Freq. (GHz)	V_{dc}(V)	I_{dc}(mA)	$P_{dc}(mW) = V_{dc} * I_{dc}$	P_{in}(dBm)	Gain (dB)	$P_{out} = P_{in} + Gain$	$\Delta\eta = \frac{P_{out}}{P_{dc}}$
[12]	2020	AI301A GaAs Tunnel Diode	0.4146	0.144	1	0.144	-43	30	-13	34.79
			0.8292					20	-23	3.48
			CG**[1]					16	-27	1.39
[11]	2019	NE3509M04 GaAs FET	2.45	1	–	–	–	11.5	–	–
[5]	2018	MBD5057-E28 Ge Tunnel Diode	5.8	0.09	0.5	0.045	-75	40	-35	0.70
[14]	2018	MBD5057-E28 Ge Tunnel Diode	5.8	0.06	0.34	0.0204	-81	31	-46	0.12
[15]	2017	NE3509M04 (Renesas) GaAs FET	1.8	1	2.4	2.4	-24.9	21.9	-3	20.87
			2.4				-24.8	13	-11.8	2.75
[16]	2017	AI301A GaAs Tunnel Diode	0.89	0.2	1	0.2	-30	17	-13	25.06
[17]	2017	AI201A GaAs Tunnel Diode	0.915	0.117	1.5	0.178	-30	13	-17	11.2
[18]	2017	2um Resonant Tunnel Diode	5.8	2*0.47	0.46	0.42	-34	8.6	-25.4	0.68
[19]	2015	MBD5057-E28 Ge Tunnel Diode	5.45	0.08	0.566	0.045	-70	34.4	-35.6	0.61
[20]	2014	BFT25A Bipolar Junction Transistor	0.915	0.755	0.431	0.325	-50	10.2	-39.8	0.03
							-40	7.7	-32.3	0.14
							-30	4.9	-25.1	0.95
[21]	2014	Bipolar Junction Transistor	0.9	0.83	0.73	0.605	-50	30	-20	1.65
							-30	14.92	-15.08	5.13
[22]	2014	BFT25A Bipolar Junction Transistor	0.9	0.83	0.8	0.664	-50	29	-21	1.20
							-20	9	-11	11.96
[23]	2014	InP 0.9um Resonant Tunnel Diode	5.7	0.36	0.173	0.125	–	10.4	–	–
[24]	2013	BPF405 (Infineon) Si BJT	5.25	2.5	0.8	2	-25	13	-12	3.15
[25]	2013	CFY30 MESFET	4.5	3	6	18	–	10.2	–	–
[26]	2013	Josephson junction	2.685	–	0.054	–	-117	30	-87	–
[27]	2012	MOSFET	4	0.8	0.15	0.12	-71.9	22.3	-49.6	0.00933
[28]	2011	NE32584 HJFET	5.8	0.7	9	6.3	–	14.8	–	–
[29]	2008	pHEMT	21	2.3	91	209.3	-75	14	-61	0
[30]	2006	pHEMT-MMIC DOIPH process	21	3	110	330	-45	14	-31	0.00024
[31]	2003	NE32584C HJFET	6.26	–	–	–	–	8.1	–	–

The reflection amplifiers can be used as modulators in backscattering RFID tags; by switching their reflection coefficients through their biasing voltage, information bits can be embedded in the reflected signal with amplitude and phase modulation [13]. Another use for the reflection amplifiers is demonstrated in [17], where a research team at the University of Illinois integrated a pair of reflection amplifiers with a four-port branch line coupler to build a bidirectional amplifier, which are used in wireless communication systems, such as half- or full-duplex radio transceivers and read/write smart RFID tags [17].

2.3 Tunnel Diode

A definition written in [17] reads: “A tunnel diode is a very heavily doped p-n junction diode with an extremely thin junction voltage barrier resulting into a quantum mechanical tunneling effect that leads to a negative input resistance at a specified bias voltage range.” The tunneling effect of the tunnel diodes was discovered in narrow Germanium p-n junctions by Leo Esaki in 1958, and it might have been predicted 25 years before [32]. The working principle of tunnel diodes is explained in detail in [19]. The ideal I-V characteristic curve of a tunnel diode is shown in Figure 2.4.

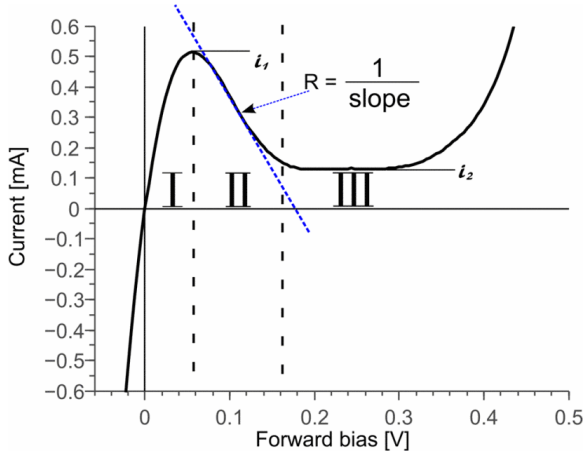

Figure 2.4. *An ideal characteristic curve of a tunnel diode*

When a low forward voltage is applied, the tunneling effect occurs (Region I of Fig. 2.4), allowing bypassing of electrons through the junction, causing a sharp rise in current to a maximum i_1. When more voltage is applied across the diode, less electrons are able to tunnel through the barrier and the current decrease to i_2 (Region II of Fig. 2.4). With larger forward bias values, the current remains around i_2 until the minority carrier injection, a phenomenon also utilized in transistors, happens (region III of Fig. 2.4). The tunnel diode thus begins to display with the exponential forward characteristic of a normal diode.

The tunnel diode is commonly biased to operate in region II, also known as the negative differential resistance (NDR) region. The small-signal negative resistance is required in Equation 2.1 in order to achieve a positive gain, i.e. a reflection coefficient higher than 1. Therefore, the reflection coefficient also depends on the DC bias voltage, enable the modulation the amplitude of the reflected signal by applying a modulated bias voltage, allowing the designs of tunneling RFID tags that are capable of not only amplifying but also modulating, as illustrated in Figure 2.5 [5].

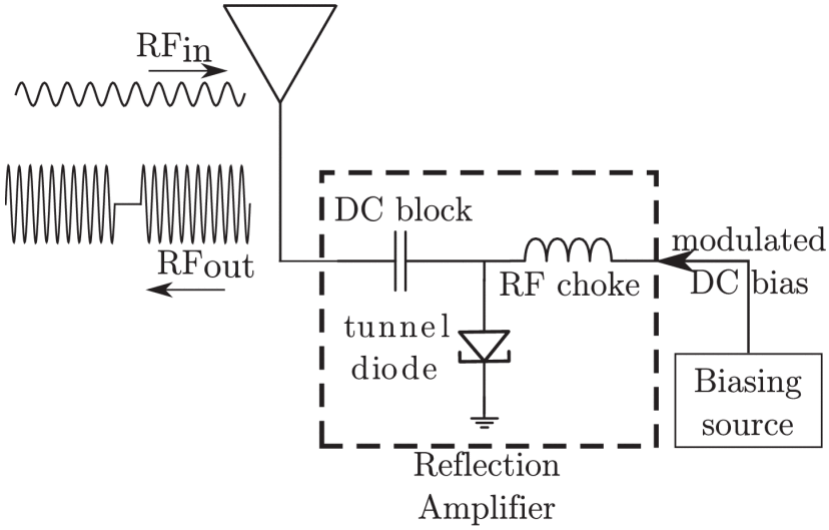

Figure 2.5. *Block diagram of a tunnel-diode based RFID reflection amplifier*

Apart from being utilized in reflection amplifier designs and RFID tags, the NDR of tunnel diodes have also been used in room-temperature Terahertz oscillators. Many other studies have explored and suggested the uses of such high frequency sources in both photonics applications such as imaging and spectroscopy, and wireless communication and radar applications [33].

Despite their potential in relevant fields, tunnel diodes are not widely available due to their difficult manufacturing process and their unstable performance. They usually consist of rare and expensive metals, such as Gallium, Germanium, and Titanium; furthermore, the quantum-mechanical theory behind their non-linear characteristics has not been fully understood. Many steps have been taken by the research community to achieve a higher-throughput and sustainable manufacturing of tunnel diodes. For example, the fabrication of organic tunnel diodes with ultra-thin Titanium Oxide (TiO_2) interfacial layers on rigid ITO substrate was studied by Pasi Heinonen [34]. Devices with 2 nm and 3 nm thick titanium layer consistently show NDR behavior. However, these devices loses their NDR characteristics when exposed to air.

3. METHODS

The design of the reflection amplifier in a circuit design software is the main focus of this thesis work. Section 3.1 goes into details on how a suitable tunnel diode model is acquired, and how a one can practically be generated from DC measurement results. The circuit is then assembled in the design software. Section 3.2 presents its schematics, as well as how the parameters are tuned together so that the circuit achieves the optimal gain at the desired center frequency.

3.1 SPICE modelling of tunnel diode

A model for the planar tunnel diode MBD5057-C18 can be found on the National Instrument Multisim, a well-known circuit simulation software used in both educational and commercial settings. However, Multisim itself does not extensively support high frequency simulation, to the best knowledge of the author. Therefore, the IV characteristics obtained in Multisim, shown in Figure 3.1, is only used as a reference. The characteristics agrees with Figure 2.4.

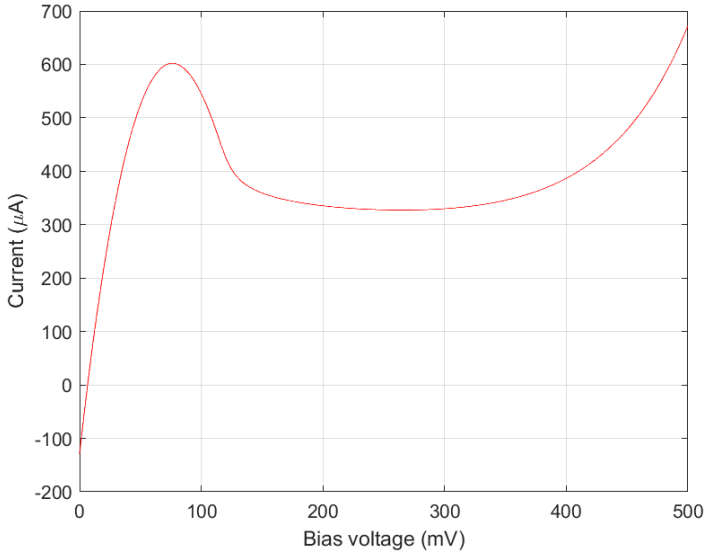

Figure 3.1. *Characteristics of MBD5057-C18 tunnel diode in Multisim*

Instead of Multisim, LTspice is used in this thesis to design and simulate the RF characteristics of the reflection amplifier, thanks to its powerful yet easy-to-use built-in tools, as well

as accessible community resources online. A model for the tunnel diode MBD5057 was downloaded from an official LTspice forum on groups.io, posted by Helmut Sennewald, its late owner. The component is modelled primarily using a diode D1, a capacitor C1, and a voltage-controlled current source (VCCS) G1 connected in parallel. D1 and C1 describe the forward-biased behavior of the diode, while G1 along with an input limiting circuit formed by R1 and D2 describe its non-linear quantum behavior. The LTspice sub-circuit model is SPICE is shown below, and Figure 3.2 illustrates the equivalent circuit. Appendix A explains the modelling of diodes in SPICE. The IV characteristic matches with the reference characteristic in Multisim, in addition to the possibilities to modify this model to converge with the DC characteristics measured from a physical tunnel diode and to add parasitic elements of the package using a parallel capacitor and a series inductor.

Listing 3.1. *LTspice subcircuit model for MBD5057*

```
.SUBCKT MBD5057 1 2
* 1 - Anode 2 - Cathode
D1 1 2 DF
C1 1 2 0.3E-12
E1 6 0 1 2 1.0
R1 5 6 100
D2 5 0 DCUT
G1 1 2 POLY(1) 5 0 -128.86E-6 20.645E-3 -164.36E-3 0.25235
.MODEL DF D (IS=260.1E-9 N=2.65 CJ0=0.001E-12)
.MODEL DCUT D (N=0.1 RS=0.001 IS=1.0E-25 CJ0=0.001E-12)
.ENDS
```

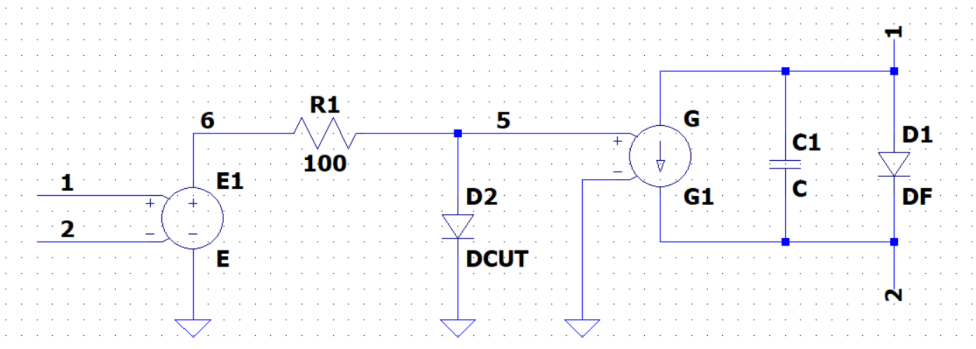

Figure 3.2. *LTspice subcircuit model schematics of the tunnel diode MBD5057*

The total current across the tunnel diode I_{tot} consists of the forward diode current I_f and the VCCS I_c, as shown in Equation 3.1.

$$I_{tot} = I_f + I_c \tag{3.1}$$

Figure 3.3 describes the elements contributing to the characteristic curve of the tunnel diode. The blue line displays the behavior of the forward diode, which grows exponentially beyond the x-limit of the graph. The red line shows the third-degree polynomial used to simulate the NDR region. The yellow line introduces the effect of the input limiting circuit preceding the VCCS, resulting in I_c. And finally, the purple line sums I_f and I_c together to form the modelled I-V characteristic of tunnel diode MBD5057.

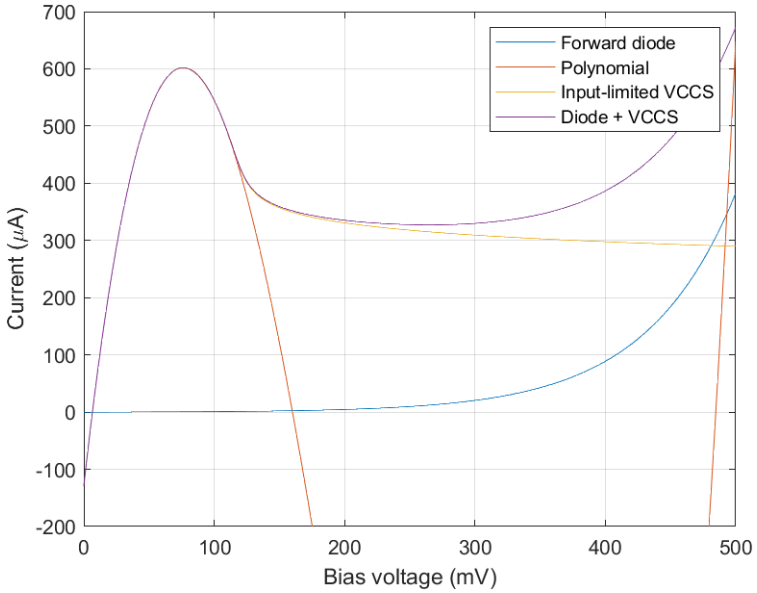

Figure 3.3. *Elements of the tunnel diode model*

Characterization of tunnel diode

By visualizing the measured DC characteristics of a tunnel diode, the following characteristic parameters can be determined for the tunnel diode SPICE model: peak current, peak voltage, valley current, valley starting voltage, and forward voltage, after which the current rises exponentially.

The low forward voltage zone leading to the NDR region can be converged with the VCCS. The polynomial can be modified to shift the peak voltage, and the zero-degree coefficient can be modified for vertical shift. Additionally, introduced by Bhattacharya et al in [35], a technique for DC convergence involving adding a weight λ to I_c in Equation 3.1 can be utilized for further fine-tuning, resulting in Equation 3.2.

$$I_{tot} = I_f + \lambda * I_c \tag{3.2}$$

At $\lambda = 0$, the VCCS is virtually removed from the subcircuit to simulate a setting without the tunnelling effect; then, this weight is increased in small steps to gradually introduce the non-linear behavior, as shown in Figure 3.4. The biggest advantage of this technique is that it separates the changes in the peak currents and the valley currents from the curve general structure.

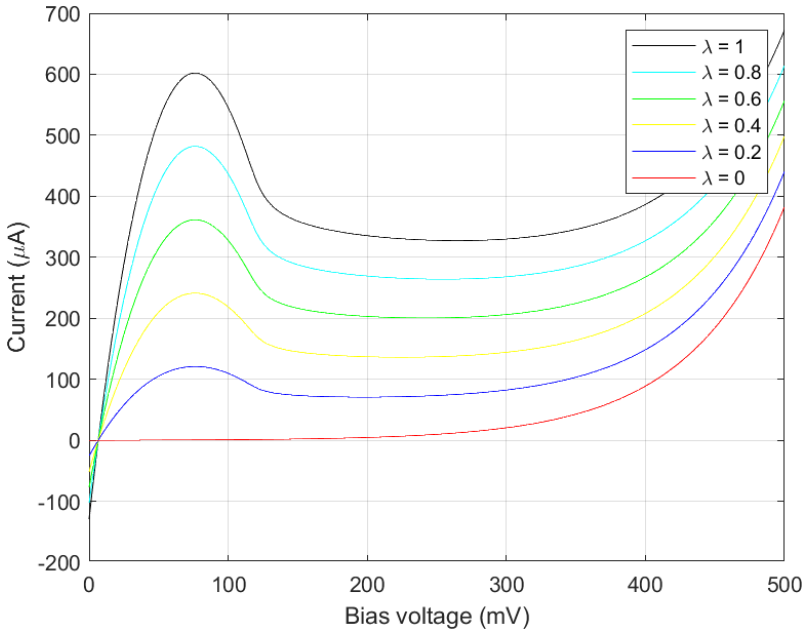

Figure 3.4. *I-V characteristic of tunnel diode MBD5057 models with different λ values*

The beginning and the ending voltage points of the valley region can be tuned by changing the emission coefficient (also known as the quality factor) of DCUT and DF. The prior sets the starting voltage of the valley, while the latter sets the end.

3.2 Circuit design

The circuit schematics is put together in LTspice as shown in Figure 3.5. Within the scope of this project, voltage sources with series resistance are used as an RF input signal source and a DC biasing source. In the deployment of reflection amplifier in RFID tags, however, antennae and ambient energy harvesting technology are implemented. The circuit consists of a matching resistor R1, a DC-block capacitor C1, an RF-choke inductor L1, as well as an MBD5057 tunnel diode D1.

The tunnel diode needs to be biased to its NDR region so that a positive reflection coefficient can be achieved. The secondary goal of DC biasing is to place the diode where its negative resistance value is the most stable, i.e. holding a relatively steady resistance despite the voltage swing caused by the input. With these requirements, the bias voltage is chosen to be 115 mV, and this achieves a stable small-signal negative resistance of about $-151\,\Omega$, as shown in Figure 3.6.

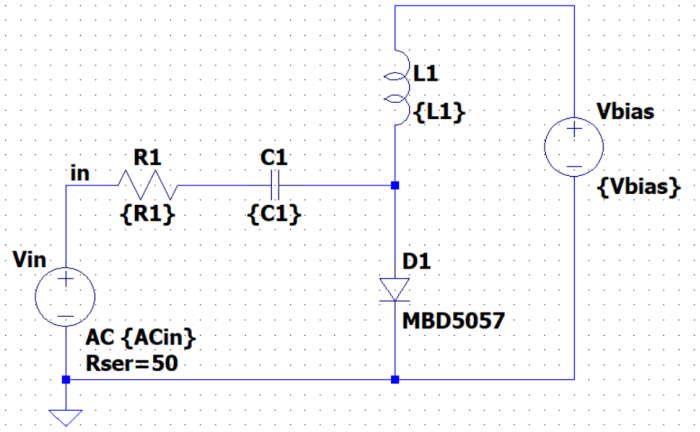

Figure 3.5. *Circuit schematics of a tunnel diode-based reflection amplifier*

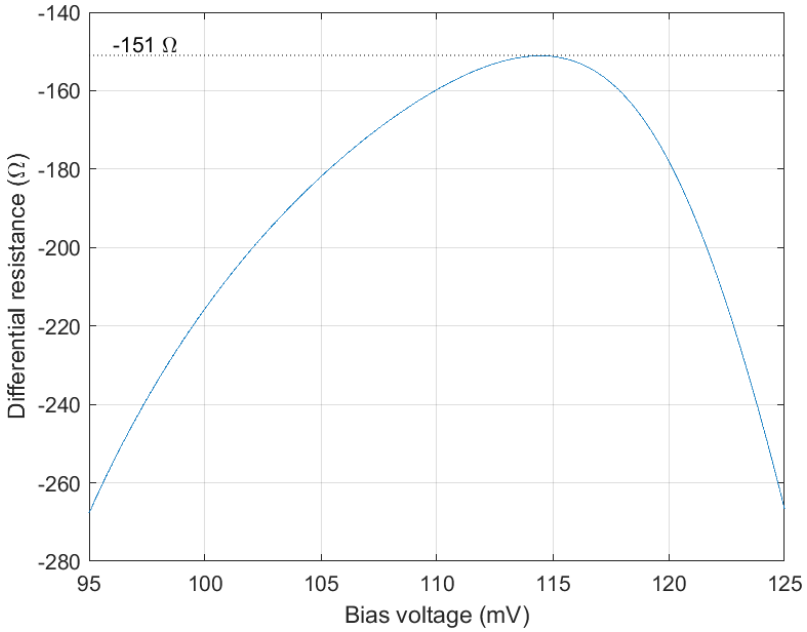

Figure 3.6. *Differential resistance against bias voltage around 115 mV*

Small-signal analysis

Small-signal analysis is a common technique to simulate and analyze circuits containing non-linear electrical components. A small-signal version of the circuit consisting of linear components, such as series and parallel resistors, capacitors, and inductors, is built and analyzed to significantly facilitate the computation of various network parameters such as input/output impedance and admittance, Y-parameters, and S-parameters. LTspice offers a built-in network analyzer that can be implemented in a small-signal frequency-sweep AC analysis. In addition to a .ac command, a .net command is included, which has the following the syntax:

.net [V(out [,ref]) | I(Rout)] <Vin | Iin> [Rin = <val>] [Rout = <val>]

The command is limited to the analysis of two-port and one-port networks. The input is

an independent source Vin or Iin. The output can be left empty in a one-port network, or specified by the voltage of a node V(out) or the current through a load I(Rout) in a two-port network. Rin and Rout are the input and output impedance, which can optionally be given to the command line if they are not already in the circuit. The reflection coefficient is calculated as the S11 parameter of the amplifier as a one-port device with voltage source Vin being both the input and output.

The analysis allows a quick visualization of the reflection gain at small-signal power level, offering a powerful tool to initialize the component values. By iterating the computation, one can capture the patterns in which the components affect the performance of the circuit as a whole, hence select optimal values. However, from a large-signal point of view, the .net analysis cannot be relied on, because a linear model does not reflects the true characteristics of the tunnel diode.

Components selection

The desired center frequency of operation of the reflection amplifier being designed in this thesis is 900 MHz, the standard UHF RFID band. R1, L1, and C1 thus have to high frequency components that are able to at the frequency range. In addition, the three components together need to satisfy the impedance matching equation $Z_{in} + Z_S = 0$ at 900 MHz in order to maximize the gain as shown in Equation 2.1. While it is possible to formulate the relationships between these values and the output gain of signal at different frequencies, because of the limited time resource, a small-signal analysis iteration-based method is taken instead.

Excluding the non-ideal parasitic elements of the inductor and the capacitor, it is rather simple to solve the matching resistance R1 for the small-signal analysis knowing every resistance value in the network:

$$Rin + (R1 + R_{D1}) = 0\,\Omega \tag{3.3}$$

Substituting known values: $Rin = 50\,\Omega$ and $R_{D1} \approx -151\,\Omega$, the resistance of $101\,\Omega$ can be chosen for R1. To confirm this value and gain more insight into its relationships with the small-signal reflection gain, R1 is gradually stepped while the response S11 is recorded. A 100 pF capacitor and a 150 nH inductor with their respective parasitic elements fulfilling the requirements as DC-block and RF-choke are initially selected, due to their availability in accessible development kits[1]. Figure 3.7 demonstrates the effect on the frequency response of slightly changing R1. Around the selected resistance point, the center frequency is not affected, but the peak gain greatly varies. Figure 3.8 further demonstrates the effect and highlights the optimal resistance at approximately $101\,\Omega$, when parasitic elements are taken into account.

[1] Johanson technology S-series 0805 capacitors and SIMID 0805-F SMT inductors

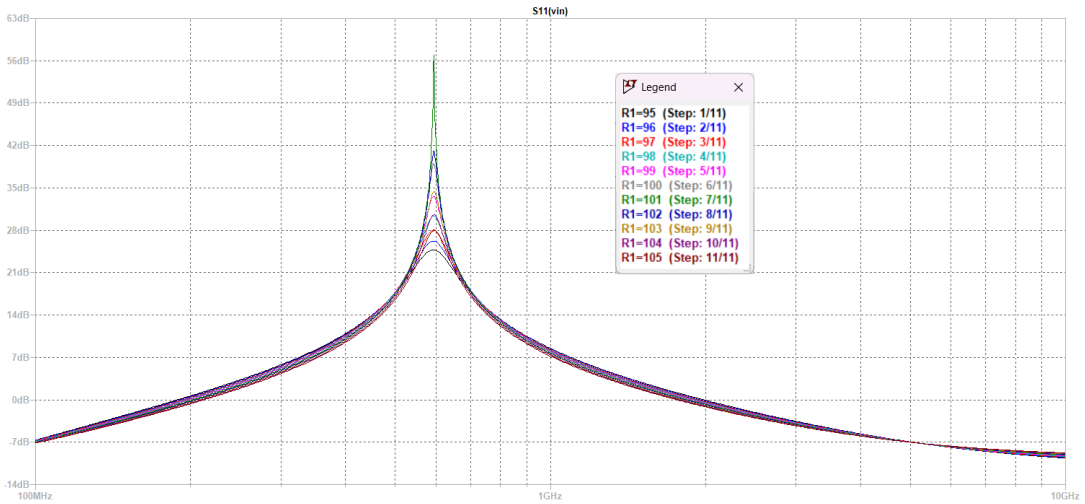

Figure 3.7. *S11 against frequency at stepping R1 values*

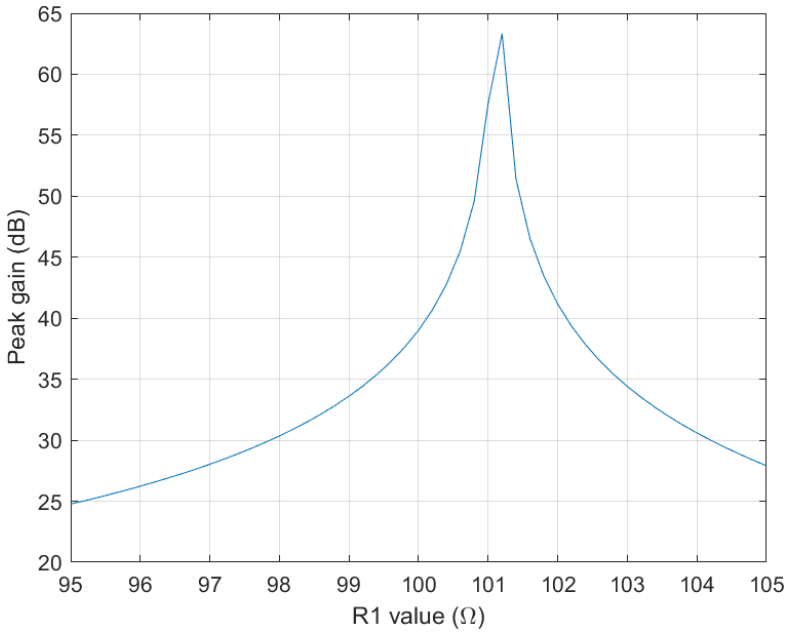

Figure 3.8. *Peak reflection coefficient against R1 (with $0.2\,\Omega$ intervals between data points)*

The effects changing C1 and L1 are demonstrated in Figure 3.9 and Figure 3.10. Tuning using the available capacitors results in a smaller and finer range possible frequency, but with a higher cost of gain; while tuning with the available inductance offer a much wider range and keep the reflection coefficient relatively high. In [5], Amato et al tune the center frequency using a tuning stub traced on the PCB instead of a packaged coil, which allows a more continuous range of possible reactance. This approach allows the even finer impedance matching by holding a capacitance value while sweeping the inductance for the highest reflection coefficient.

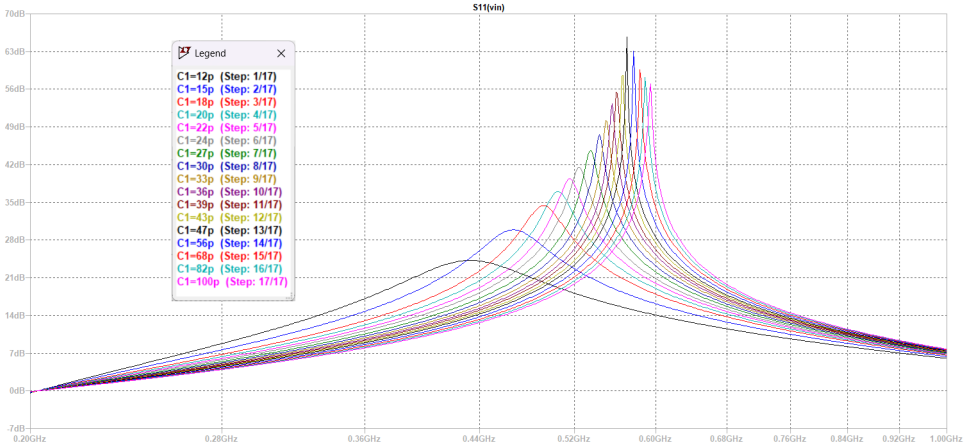

Figure 3.9. *S11 against frequency for different available capacitors (L1 = 150 nH)*

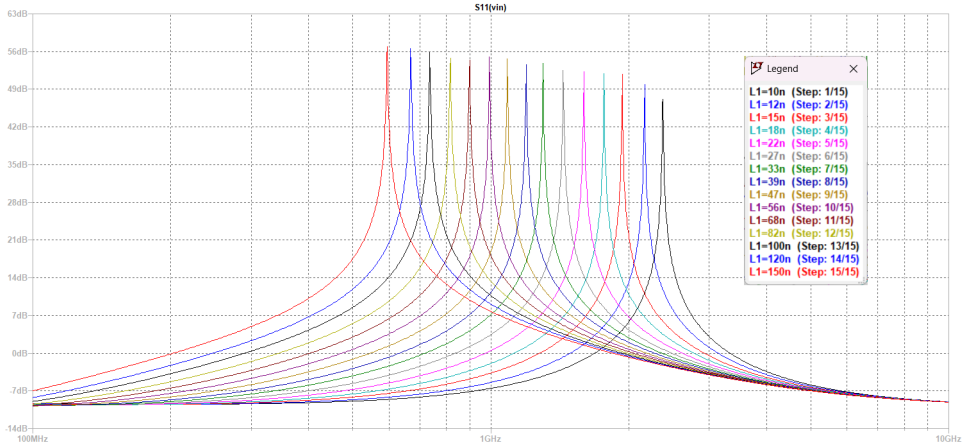

Figure 3.10. *S11 against frequency for different available inductors (C1 = 100 pF)*

With the previously found terminating resistance $R1 = 50\,\Omega$, the following L1-C1 pairings satisfy the center frequency of 900 MHz: 68 nH with 100 pF; and 56 nH with 12 pF. Figure 3.11 plot the small-signal responses of the amplifiers in the UHF band (870 - 930 MHz).

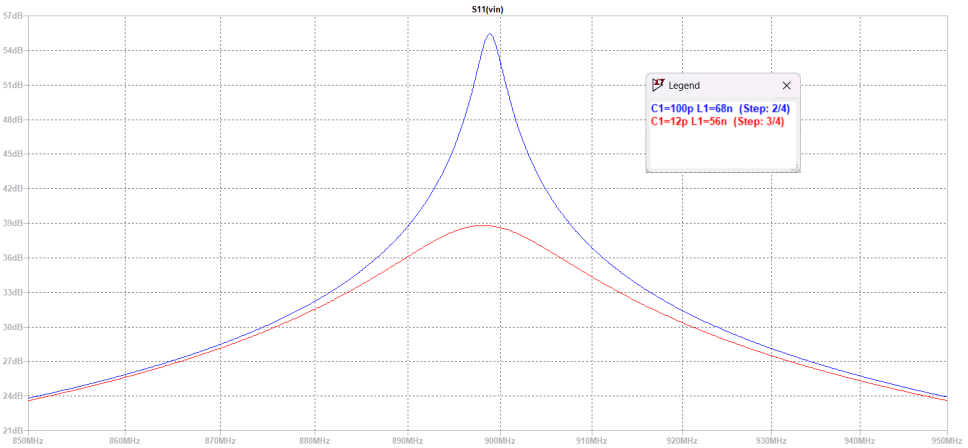

Figure 3.11. *S11 against frequency for 900-MHz-centered reflection amplifiers*

On first glance, it seems that the first pairing results in a much higher gain, but an AC analysis stepping over R1 values, as illustrated in Figure 3.12 tells a different story. Even in small-signal analysis, the drastic difference in the DC-block capacitance C1 causes a change in the matching resistance. For unknown reasons, there is a relationship between the choice of inductors and capacitors and the termination resistance, which has to be kept in mind. It seems that the decreasing of the capacitance has a much more significant effect than the decreasing of the inductance.

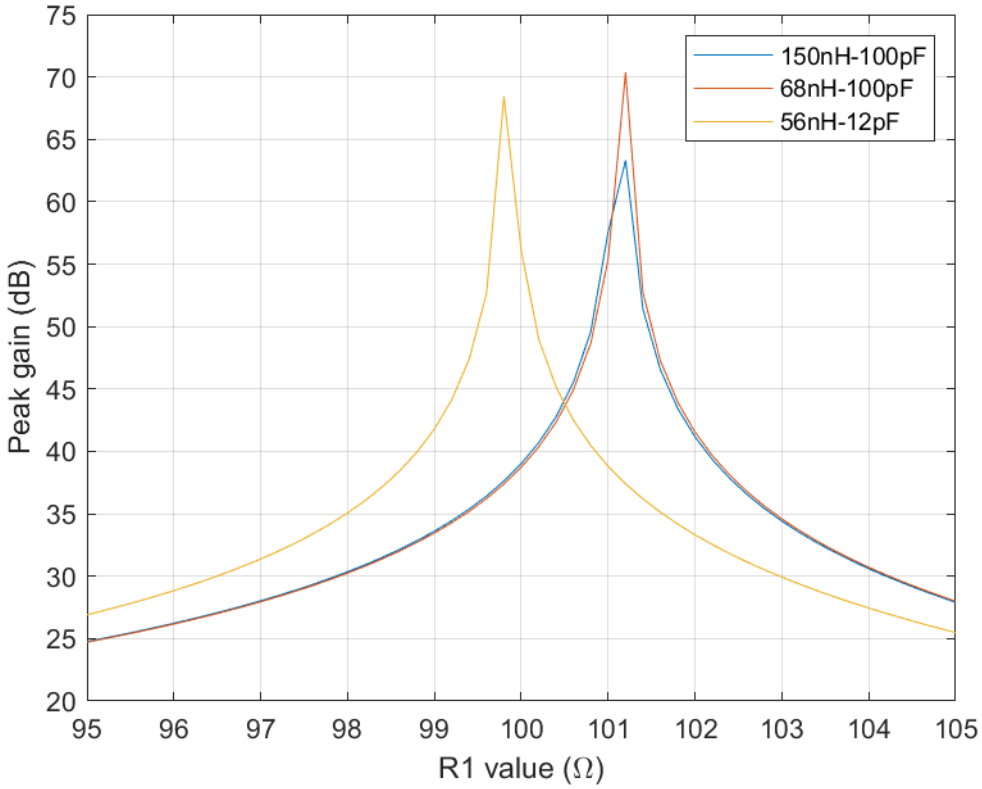

Figure 3.12. *Peak reflection coefficient against R1 (with $0.2\,\Omega$ intervals between data points) for different component selections*

4. SIMULATIONS

Although the AC analysis revealed some powerful reflection amplifier designs with gains potentially being as high as 60 dB, it is yet only the case for linear small-signal models created for the analysis. The large-signal behaviors of the circuit, on the other hand, are non-linear. Without the time resource for building prototypes and measurement with powerful equipment such as the vector network analyzer or the spectrum analyzer, this thesis utilizes simulation software to ensure and record the functionality of the design. Section 4.1 introduces available tools, and propose a simulation setup that can capture important large-signal operational parameters. Section 4.2 presents the results and their implications.

4.1 Simulation setup

In LTspice, the command .tran is used to directly simulate a circuit over a specified amount of time, much similar to the operation of an oscilloscope, but without the possibility of real-time interaction. The syntax is shown below:

.tran <Tstep> <Tstop> [Tstart [dTmax]] [modifiers]

This command perform a nonlinear transient analysis, computing what happens when the circuit under test is powered up. Tstep is the waveform plotting increments, and is also used as an initial step-size guess. This value is usually set to zero because LTspice uses waveform compression. Tstop is the duration of the transient analysis. The analysis always start at time zero, even when Tstart is specified, which means that the data between zero and Tstart not being saved. The final parameter dTmax specify the maximum time step to take while performing calculations. Optional transient analysis modifiers can be added at the end to further manage waveform data saving and simulation timings; however, this thesis does not delve into the use these tools.[1]

Figure 4.1 illustrate the transient simulation setup for the reflection amplifier. A circulator isolates the output reflection signal to make visualization and comparison easier. Its model is downloaded from LTspice group.io forum, and is included in Appendix B. Enclosed in the green box, a sinusoidal test signal of frequency **Fin** and peak-to-peak

[1] LTspiceHelp » LTspice » LTspice® » Dot Commands » .TRAN – Do a Nonlinear Transient Analysis

amplitude **RFin** is fed to port 1 of the circulator, and exits at port 2 as input to the reflection amplifier (RA), enclosed in the yellow box. Enclosed in the red box at port 3 of the circulator, the reflected signal is isolated and connected to a load resistor with the same input series resistance **Rin** emulating the antenna impedance.

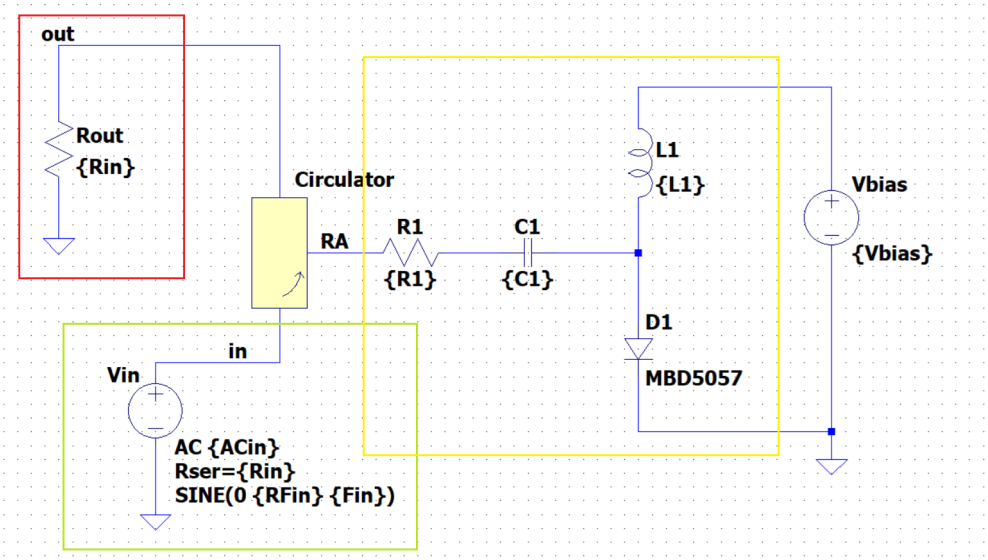

Figure 4.1. *Transient simulation setup with a circulator*

The results obtained from a transient analysis are voltage and current values plotted against time. Because signals at a specific frequency of 900 MHz are dealt with in this case, these waveforms do not offer much valuable information on their own. Instead, conversion into the frequency domain through the mean of Fourier transform is required. LTspice has a powerful built-in FFT (Fast Fourier Transform) algorithm that allows an arbitrary number of data points, i.e. not limited to powers of 2[2]. However, plotting an entire Fourier transform takes a lot of computing power and time, which limits the resolution with which the input RF voltage can be stepped. Instead, the more direct command .four is used, with the following syntax:

.four <frequency> [Nharmonics] [Nperiods] <data trace1> [<data trace2> ...]

This command is computes a specified Fourier frequency component of (some) data traces after a transient analysis. Optionally, Nharmonics and Nperiods values can be supplied to specify the number of harmonics to be included, and the number of periods in which the Fourier analysis is performed. With the example command statements below and setting RFin = 10u, Figure 4.2 shows the results formatted in LTspice error log. In the .four statement, Nperiods equals -1 means that the Fourier analysis is applied over the entire simulating duration; and the data saving start time is set to 50n so that the output waveform is stable.

[2]LTspiceHelp » Waveform Viewer » Waveform Arithmetic

.tran 0 1050n 50n 5p
.four 900meg 9 -1 V(out)

N-Period=900.00
Fourier components of V(out)
DC component:-2.70137e-10

Harmonic Number	Frequency [Hz]	Fourier Component	Normalized Component	Phase [degree]	Normalized Phase [deg]
1	9.000e+8	3.072e-4	1.000e+0	95.07°	0.00°
2	1.800e+9	4.721e-7	1.537e-3	100.59°	5.52°
3	2.700e+9	1.423e-7	4.633e-4	131.68°	36.62°
4	3.600e+9	6.175e-9	2.010e-5	54.93°	-40.13°
5	4.500e+9	1.322e-7	4.303e-4	-72.69°	-167.75°
6	5.400e+9	1.259e-8	4.098e-5	-74.57°	-169.64°
7	6.300e+9	1.723e-7	5.608e-4	125.87°	30.81°
8	7.200e+9	1.056e-8	3.436e-5	157.89°	62.83°
9	8.100e+9	5.588e-8	1.819e-4	-37.78°	-132.85°

Partial Harmonic Distortion: 0.176403%
Total Harmonic Distortion: 0.222258%

Figure 4.2. *Fourier analysis results in LTspice error log*

The unit of "Fourier Component" is volt (V). The voltage gain can be calculated by dividing it by the input RF voltage RFin, and then converted to power gain in dB. By iterating this process, the reflected signal gain can be plotted against the input power, which is obtained by converting RFin to dBm.

4.2 Results

Figure 4.3 shows the large-signal performance of the reflection amplifier designs with resistance matched using small-signal analysis in the previous chapter. Along with other factors, as suggested in Equation 2.1, Pin also heavily affects the amplification, as the operating area of the tunnel diode becomes larger.

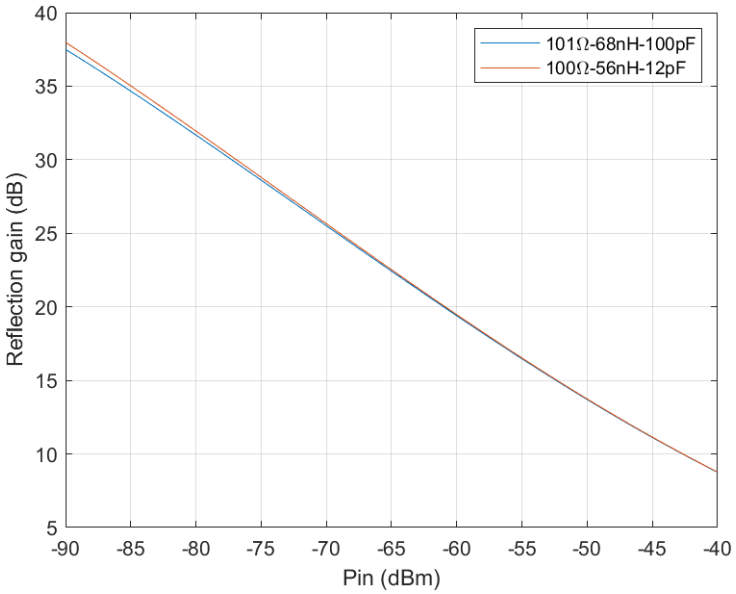

Figure 4.3. *Reflection gain against input power with reflection amplifier matched using small-signal analysis*

The reflection amplifier, therefore, has to be matched at an operating input power. Through iterations, ideal matching resistance values are found, and shown in Table 4.1; and Figure 4.4 and 4.5 illustrates the increase in gain obtained by large-signal resistance matching.

Table 4.1. *Terminating resistance matching at different input power*

P_{in}	**68nH-100pF**	**56nH-12pF**
Small-signal	$101\,\Omega$	$100\,\Omega$
-80 dBm	$119\,\Omega$	$111\,\Omega$
-65 dBm	$143\,\Omega$	$138\,\Omega$
-50 dBm	$223\,\Omega$	$187\,\Omega$

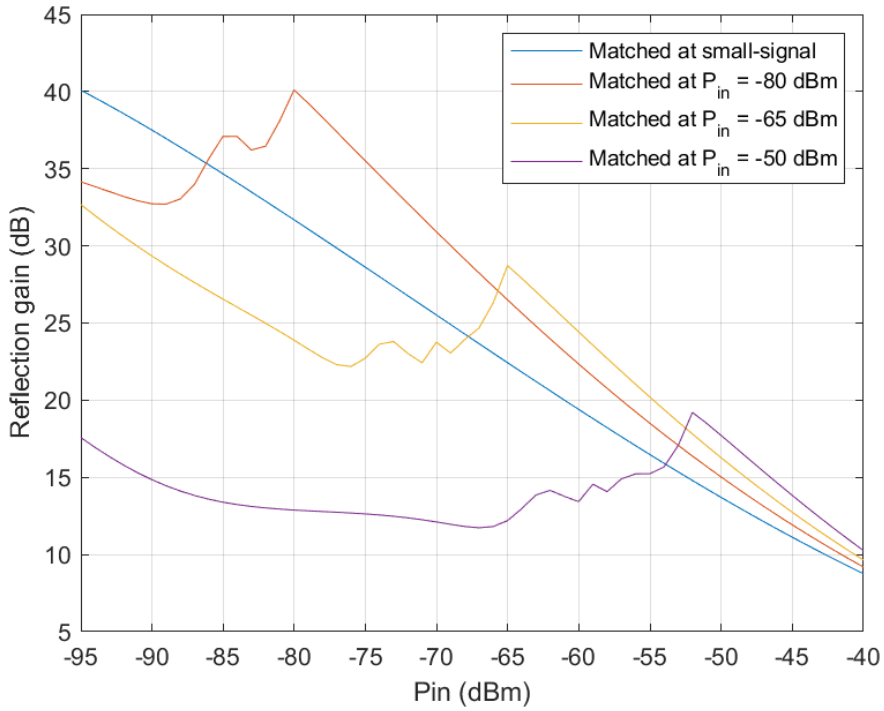

Figure 4.4. *Reflection gain against input power of 68nH-100pF circuits, terminating at different input levels*

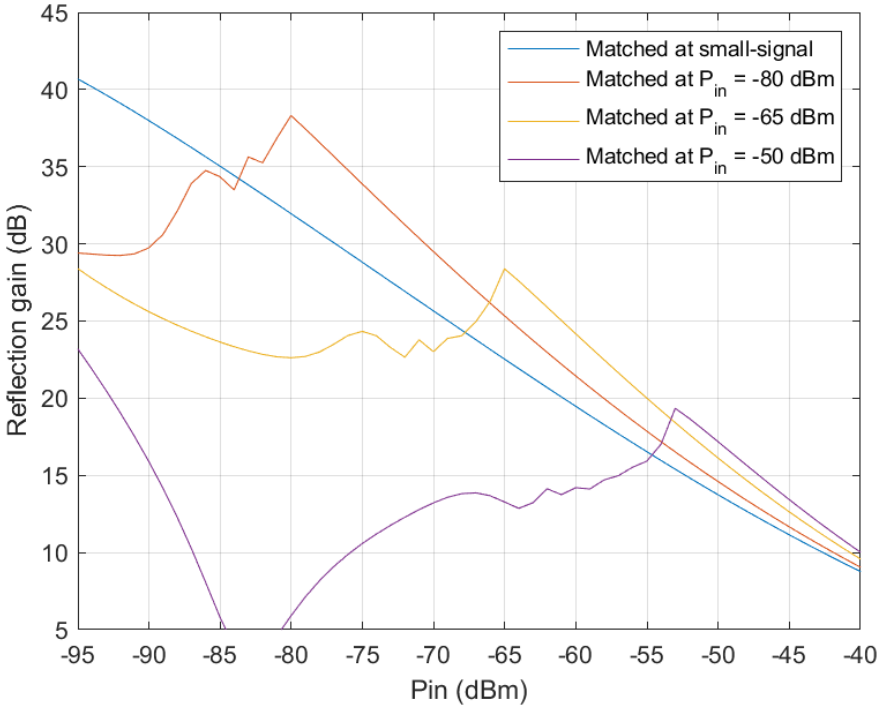

Figure 4.5. *Reflection gain against input power of 56nH-12pF circuits, terminating at different input levels*

The frequency responses to the reflection amplifier can be plotted by keeping the input power constant while sweeping through possible input frequencies, as shown in Figure 4.6 for the 143Ω-68nH-100pF (#1) and the 138Ω-56nH-12pF (#2) reflection amplifiers. The frequency deviation, forming the seemingly coincident sharp cut-offs at 900 MHz, means that the reactance, along with the resistance, has to be matched at the desired operating power. However, due to the lack of time resource and the limited available values of inductance and capacitance, this process is reserved for later stages of the research.

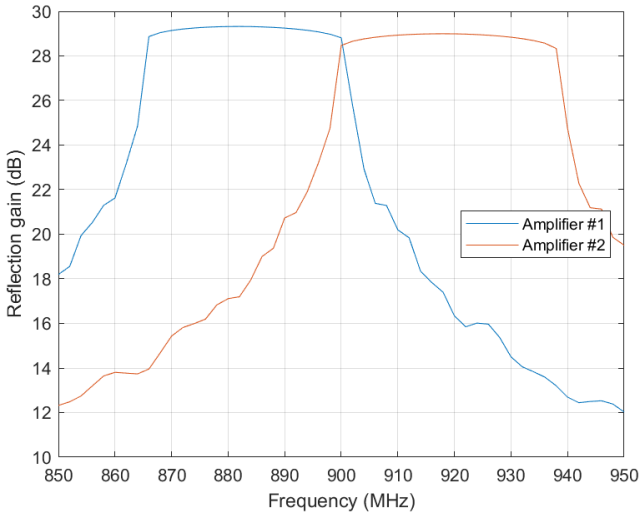

Figure 4.6. *Amplitude response at UHF band, Pin = -65 dBm*

5. CONCLUSION

This thesis has introduced the background theory and works related to the reflection amplifier, sketched a component modelling and circuit designing process, and finally made assessments and provided necessary improvements to be done in the future regarding the circuit design. Even though a conclusive design process has neither been proposed nor verified in this work, a proper starting point for future research regarding the tunnel diode-based reflection amplifier has been made.

The design process starts with the IV characterizations of a tunnel diode, which is then converged by a SPICE model. A DC bias voltage across the tunnel diode is then chosen based on its model, in order to maintain a stable negative differential resistance. Next, small-signal analyses are iterated over different circuit parameters to capture the effects of each elements, and choose a set of optimal values for the desired resonant frequency. The circuit is then inspected with large-signal analyses in time-domain together with Fourier transform. The initial small-signal-based values can be further optimized for gain and frequency alignment.

It is shown in the simulation that with the correct tuning of circuit parameters, and minimizing and including of non-ideal factor in the simulation, a reflection amplifier utilizing the tunnelling effect having high gain up to 40 dB for 900 MHz signal at RF input power as low as -80 dBm. However, these optimistic numbers only apply for a specific and ideal tunnel diode model, which is, by nature, an extremely unpredictable component. Despite the its huge potential in RFID technology, there are still a lot more to learn about the tunnel diode, regarding both its characterization and manufacturing, which will no doubt pose many challenges for future studies on this topic.

REFERENCES

[1] Want, R. An introduction to RFID technology. *IEEE Pervasive Computing* 5.1 (2006), pp. 25–33. DOI: 10.1109/MPRV.2006.2.

[2] Kim, S., Georgiadis, A. and Tentzeris, M. M. Design of inkjet-printed RFID-based sensor on paper: Single-and dual-tag sensor topologies. eng. *Sensors (Basel, Switzerland)* 18.6 (2018), pp. 1958–. ISSN: 1424-8220.

[3] Sharif, A., Ouyang, J., Raza, A., Imran, M. A. and Abbasi, Q. H. Inkjet-printed UHF RFID tag based system for salinity and sugar detection. eng. *Microwave and optical technology letters* 61.9 (2019), pp. 2161–2168. ISSN: 0895-2477.

[4] Boyer, C. and Roy, S. Backscatter Communication and RFID: Coding, Energy, and MIMO Analysis. *IEEE Transactions on Communications* 62.3 (2014), pp. 770–785. DOI: 10.1109/TCOMM.2013.120713.130417.

[5] Amato, F., Peterson, C. W., Degnan, B. P. and Durgin, G. D. Tunneling RFID Tags for Long-Range and Low-Power Microwave Applications. eng. *IEEE Journal of Radio Frequency Identification* 2.2 (2018), pp. 93–103. ISSN: 2469-7281.

[6] *Laboratory for Future Electronics*. URL: https://research.tuni.fi/lfe/ (visited on 04/06/2024).

[7] Ambient Backscatter Communications: A Contemporary Survey. eng. *IEEE Communications surveys and tutorials* 20.4 (2018), pp. 2889–2922. ISSN: 1553-877X.

[8] Advances in Wirelessly Powered Backscatter Communications: From Antenna/RF Circuitry Design to Printed Flexible Electronics. eng. *Proceedings of the IEEE* 110.1 (2022), pp. 171–192. ISSN: 0018-9219.

[9] Liu, W., Huang, K., Zhou, X. and Durrani, S. Next generation backscatter communication: systems, techniques, and applications. eng. *EURASIP journal on wireless communications and networking* 2019.1 (2019), pp. 1–11. ISSN: 1687-1499.

[10] Niu, J.-P. and Li, G. Y. An Overview on Backscatter Communications. *Journal of Communications and Information Networks* 4.2 (2019), pp. 1–14. DOI: 10.23919/JCIN.2019.8917868.

[11] Khaledian, S., Farzami, F., Smida, B. and Erricolo, D. Two-Way Backscatter Communication Tag Using a Reflection Amplifier. eng. *IEEE microwave and wireless components letters* 29.6 (2019), pp. 421–423. ISSN: 1531-1309.

[12] Gumber, K., Dejous, C. and Hemour, S. Harmonic Reflection Amplifier for Widespread Backscatter Internet-of-Things. eng. *IEEE transactions on microwave theory and techniques* 69.1 (2021), pp. 774–785. ISSN: 0018-9480.

[13] Chan, P. and Fusco, V. An 8- to 12-GHz wideband negative resistance reflection amplifier. eng. *Microwave and optical technology letters* 54.3 (2012), pp. 553–555. ISSN: 0895-2477.

[14] Amato, F., Torun, H. M. and Durgin, G. D. RFID Backscattering in Long-Range Scenarios. *IEEE Transactions on Wireless Communications* 17.4 (2018), pp. 2718–2725. DOI: 10.1109/TWC.2018.2801803.

[15] Farzami, F., Khaledian, S., Smida, B. and Erricolo, D. Reconfigurable Dual-Band Bidirectional Reflection Amplifier With Applications in Van Atta Array. eng. *IEEE transactions on microwave theory and techniques* 65.11 (2017), pp. 4198–4207. ISSN: 0018-9480.

[16] Farzami, F., Khaledian, S., Smida, B. and Erricolo, D. Ultra-low power reflection amplifier using tunnel diode for RFID applications. eng. *2017 IEEE International Symposium on Antennas and Propagation & USNC/URSI National Radio Science Meeting*. IEEE, 2017, pp. 2511–2512. ISBN: 9781538632840.

[17] Khaledian, S., Farzami, F., Erricolo, D. and Smida, B. A Full-Duplex Bidirectional Amplifier With Low DC Power Consumption Using Tunnel Diodes. eng. *IEEE microwave and wireless components letters* 27.12 (2017), pp. 1125–1127. ISSN: 1531-1309.

[18] Lee, J. and Yang, K. RF Power Analysis on 5.8 GHz Low-Power Amplifier Using Resonant Tunneling Diodes. eng. *IEEE microwave and wireless components letters* 27.1 (2017), pp. 61–63. ISSN: 1531-1309.

[19] Amato, F., Peterson, C. W., Degnan, B. P. and Durgin, G. D. A 45 uW bias power, 34 dB gain reflection amplifier exploiting the tunneling effect for RFID applications. eng. *2015 IEEE International Conference on RFID (RFID)*. IEEE, 2015, pp. 137–144. ISBN: 9781479919376.

[20] Kimionis, J., Georgiadis, A., Collado, A. and Tentzeris, M. M. Enhancement of RF Tag Backscatter Efficiency With Low-Power Reflection Amplifiers. eng. *IEEE transactions on microwave theory and techniques* 62.12 (2014), pp. 3562–3571. ISSN: 0018-9480.

[21] Kimionis, J., Tentzeris, M. M., Georgiadis, A. and Collado, A. Inkjet-printed reflection amplifier for increased-range Backscatter radio. eng. *2014 44th European Microwave Conference*. European Microwave Association, 2014, pp. 5–8. ISBN: 2874870358.

[22] Kimionis, J., Georgiadis, A., Kim, S., Collado, A., Niotaki, K. and Tentzeris, M. M. An enhanced-range RFID tag using an ambient energy powered reflection amplifier. eng. *2014 IEEE MTT-S International Microwave Symposium (IMS2014)*. IEEE, 2014, pp. 1–4. ISBN: 1479938696.

[23] Lee, J., Lee, J. and Yang, K. Reflection-Type RTD Low-Power Amplifier With Deep Sub-mW DC Power Consumption. eng. *IEEE microwave and wireless components letters* 24.8 (2014), pp. 551–553. ISSN: 1531-1309.

[24] Chan, P. and Fusco, V. Full duplex reflection amplifier tag. eng. *IET microwaves, antennas & propagation* 7.6 (2013), pp. 415–420. ISSN: 1751-8725.

[25] Lazaro, A., Ramos, A., Villarino, R. and Girbau, D. Time-Domain UWB RFID Tag Based on Reflection Amplifier. eng. *IEEE antennas and wireless propagation letters* 12 (2013), pp. 520–523. ISSN: 1536-1225.

[26] Vesterinen, V., Hassel, J. and Seppa, H. Tunable Impedance Matching for Josephson Junction Reflection Amplifier. eng. *IEEE transactions on applied superconductivity* 23.3 (2013), pp. 1500104–1500104. ISSN: 1051-8223.

[27] Bousquet, J.-F., Magierowski, S. and Messier, G. G. A 4-GHz Active Scatterer in 130-nm CMOS for Phase Sweep Amplify-and-Forward. eng. *IEEE transactions on circuits and systems. I, Regular papers* 59.3 (2012), pp. 529–540. ISSN: 1549-8328.

[28] Chan, P. and Fusco, V. Bi-static 5.8GHz RFID range enhancement using retrodirective techniques. *2011 41st European Microwave Conference*. 2011, pp. 976–979. DOI: 10.23919/EuMC.2011.6101753.

[29] Cantu, H. I., Fusco, V. F. and Simms, S. Microwave reflection amplifier for detection and tagging applications. eng. *IET microwaves, antennas & propagation* 2.2 (2008), pp. 115–119. ISSN: 1751-8725.

[30] Cantu, H. and Fusco, V. A 21 GHz reflection amplifier MMIC for retro-directive antenna and RFID applications. eng. *IET Seminar Digest*. Vol. 2006. 11593. Stevenage: Inst. of Eng. and Technol, 2006, pp. 66–70. ISBN: 0863417191.

[31] Chung, S. J., Chen, S. M. and Lee, Y. C. A novel bi-directional amplifier with applications in active Van Atta retrodirective arrays. eng. *IEEE transactions on microwave theory and techniques* 51.2 (2003), pp. 542–547. ISSN: 0018-9480.

[32] Esaki, L. New phenomenon in narrow germanium p-n junctions [3]. eng. *Physical review* 109.2 (1958), pp. 603–604. ISSN: 0031-899X.

[33] Asada, M. and Suzuki, S. Terahertz emitter using resonant-tunneling diode and applications. eng. *Sensors (Basel, Switzerland)* 21.4 (2021), pp. 1–20. ISSN: 1424-8220.

[34] Heinonen, P. P. *Fabrication of organic tunnel diodes with ultra-thin TiO2 interfacial layers*. eng. Materiaaliopin laitos - Department of Materials Science, 2015.

[35] Bhattacharya, M. and Mazumder, P. Augmentation of SPICE for simulation of circuits containing resonant tunneling diodes. *IEEE Transactions on Computer-Aided Design of Integrated Circuits and Systems* 20.1 (2001), pp. 39–50. DOI: 10.1109/43.905673.

APPENDIX A: SPICE MODELLING OF DIODE

Table A.1 lists the model parameters that can be provided. The DC characteristics of the diode are determined by the parameters **IS** and **N**. An ohmic resistance, **RS**, is included. Charge storage effects are modeled by a transit time, **TT**, and a nonlinear depletion layer capacitance which is determined by the parameters **CJO**, **VJ**, and **M**. The temperature dependence of the saturation current is defined by the parameters **EG**, the energy and **XTI**, the saturation current temperature exponent. Reverse breakdown is modeled by an exponential increase in the reverse diode current and is determined by the parameters **BV** and **IBV** (both of which are positive numbers).

Table A.1. *Diode model parameters*

Name	*Parameter*	*Units*	*Default*	*Typical*
IS	Saturation current	A	10^{-14}	10^{-14}
RS	Ohmic series resistance	Ω	0	3
N	Emission coefficient	-	1	1
TT	Transit time	s	0	10^{-9}
CJO	Zero-bias junction capacitance	F	0	$3 * 10^{-12}$
VJ	Junction potential	V	1	0.8
M	Grading coefficient	-	0.5	0.5
EG	Energy gap	eV	1.11	1.11
XTI	Saturation current temperature exponent	-	3.0	3.0
KF	Flicker noise coefficient	-	0	-
AF	Flicker noise exponent	-	1	-
FC	Coefficient for forward-bias depletion capacitance formula	-	0.5	-
BV	Reverse breakdown voltage	V	$\inf$	80
IBV	Current at breakdown voltage	A	10^{-3}	$2 * 10^{-3}$
TNOM	Temperature at which parameters were measured	$^{\circ}C$	27	27

SPICE command: **.MODEL** *model name* **D** (*model parameters*)

Some examples:

*Diode small power
.MODEL 1N3879 D(IS=1.6e-18 BV=50 IBV=10u M=0.27 CJO=100p RS=9m TT=0.3u)

*Switching diode
.MODEL 1N4148 D(IS=0.1p RS=16 CJO=2p TT=12n BV=100 IBV=0.1p)

*Rectifier diode with 400 V breakdown voltage and 25 A
.MODEL 1N3494 D(IS=5E-14 BV=400 IBV=0.001 M=0.84 CJO=1.5NF RS=3m TT=8u)

*Germanium diode
.MODEL 1N5817 D(N=1.2 IS=20U RS=.08 EG=.69 XTI=2 CJO=200p BV=25 IBV=.01m
+ M=.523 VJ=2)

*Zener diode, 6.8 V
.MODEL 1N754 D(IS=1E-15 RS=.25 CJO=150p M=.55 VJ=.75 ISR=2n BV=6.8 IBV=20m)

*Variable-capacitance diode
.MODEL MV2201 D(IS=1p CJO=15p M=.4261 VJ=.75 FC=.5 BV=25 IBV=10u)

APPENDIX B: CIRCULATOR SPICE MODEL

The following equivalent subcircuit, illustrated in Figure B.1 , is used to model the circulator used in the setup in Figure 4.1. The subcircuit is download from LTspice group.io forum, posted by Helmut Sennewald. A SPICE code is written based on the subcircuit, a simple three-port schematic symbol is designed, and both are implemented in the transient simulation setup.

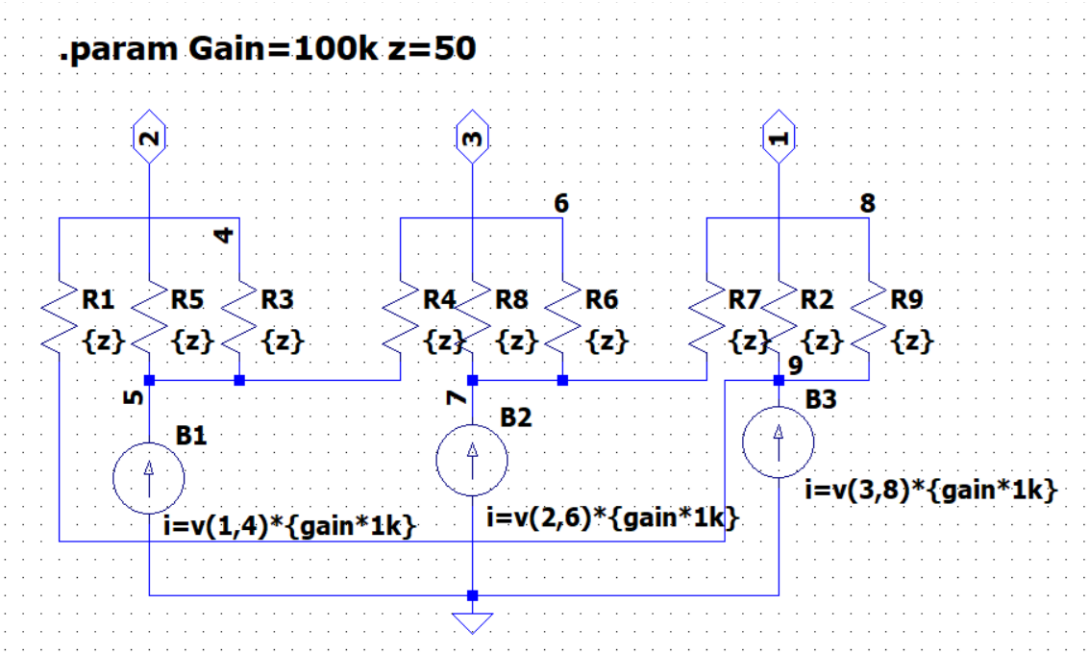

Figure B.1. *Subcircuit modelling of the circulator*